Integrated Approach to Study the Dehydration Kinetics of Nitrofurantoin Monohydrate

VISHAL KORADIA,[1] HEIDI LOPEZ DE DIEGO,[2] MICHIEL RINGKJØBING ELEMA,[3] JUKKA RANTANEN[1]

[1]Faculty of Pharmaceutical Sciences, Department of Pharmaceutics and Analytical Chemistry, University of Copenhagen, Copenhagen, Denmark

[2]H. Lundbeck A/S, Preformulation, Copenhagen, Denmark

[3]H. Lundbeck A/S, Pharmaceutical Development, Copenhagen, Denmark

Received 8 September 2009; accepted 23 April 2010

Published online 23 June 2010 in Wiley InterScience (www.interscience.wiley.com). DOI 10.1002/jps.22244

ABSTRACT: There is a need for thorough knowledge of solid-state transformations in order to implement quality by design (QbD) methodology in drug development. The present study was aimed at gaining a mechanistic understanding of the dehydration of nitrofurantoin monohydrate II (NF-MH). The dehydration was studied using thermogravimetric analysis (TGA), differential scanning calorimetry (DSC), hot-stage microscopy (HSM), and variable temperature X-ray powder diffraction (VT-XRPD). Isothermal TGA data were used to study dehydration kinetics using model-fitting and model-free approaches. Model-fitting analysis indicated a good fit for several models derived from nucleation–growth and/or geometric contraction mechanisms. However, based on visual observations during HSM, Avrami–Erofeyev equations A3 and A4, indicating nucleation–growth phenomenon, were found to be the most suitable kinetic models. HSM showed initiation of dehydration with random nucleation, and nuclei coalesced with the progress of dehydration reaction. VT-XRPD revealed formation of anhydrate β form on dehydration of NF-MH. The phenomenon of random nucleation is justified based on the crystal structure of NF-MH, which showed presence of water molecules in an isolated manner, prohibiting directional dehydration. It was found that supplementary information from HSM and VT-XRPD can be valuable to gain a better understanding of dehydration from formal solid-state kinetics analysis. © 2010 Wiley-Liss, Inc. and the American Pharmacists Association J Pharm Sci 99:3966–3976, 2010

Keywords: hydrate; dehydration; thermogravimetric analysis; X-ray diffractometry; solid-state stability; transformation; solid-state kinetics; nitrofurantoin

INTRODUCTION

Many pharmaceutically relevant substances exist as hydrates, and survey within European Pharmacopoeia indicated that 29% of the compounds are known to form hydrates.[1] The potential impact of changes in the hydrate/anhydrate state of the crystalline drug substances and excipients exists throughout the drug development process.[2] The occurrence and behavior of hydrates has received increasing attention during the last decade, primarily due to the potential impact of hydrates on the development process and dosage form performance.[3,4] Owing to the extensive hydrogen bonding capability of water, it plays an important role in the stability of the crystal structure.[5] In general, breakage of hydrogen bond network due to dehydration can lead to conversion of hydrate to a lower hydrate state, anhydrate or amorphous/melt, which can subsequently crystallize.[6] The hydrate formation/dehydration may occur during various unit operations such as crystallization,[7] wet granulation,[8] pelletization,[9] drying,[10,11] milling,[12] lyophilization,[13] or during normal storage of the finished product.[14,15] Because the phase transition on dehydration is accompanied by a change in the physicochemical properties, it is important to understand the mechanisms of these transitions, the experimental and environmental conditions under which these take place, and their rate constant under various conditions.[16] An understanding of the critical factors involved in the dehydration of hydrate can be of use as a guide both during preformulation and later

Correspondence to: Jukka Rantanen (Telephone: 45-35-33-65-85; Fax: 45-35-33-60-30; E-mail: jtr@farma.ku.dk)

Journal of Pharmaceutical Sciences, Vol. 99, 3966–3976 (2010)

in the development process. A structured approach using formal solid-state kinetics is one way of gaining an understanding of the dehydration reaction, and this approach has attracted pharmaceutical researchers since the 1970s.[17,18] Since then, many other studies have been reported on hydrates and have contributed towards an understanding of the dehydration process.[16,19–23] Moreover, dehydration itself constitutes an important class of reactions which has contributed significantly to the provision of the theoretical foundation for the understanding of solid-state reactions.[24] A classification scheme of dehydration based on structural and kinetic criteria has been proposed by Galwey.[25] Petit and Coquerel[26] have presented another model based on the water release pathways and possible reorganization of the dehydration product. Dehydration of crystalline solids represents an important group of heterogeneous solid-state reactions, and dehydration kinetics analysis can be performed by either model-fitting or model-free methods.[25,27,28] Unlike the rate laws in homogenous kinetics, which usually depend on the reaction order (i.e., first, second, etc.), a rate law for an elementary solid-state reaction like dehydration could depend on factors such as rate of nuclei formation, interface advance, diffusion, and/or geometrical shape of the solid particles. These factors have led to evolution of several kinetic models. These are presented in Table 1.

Model-fitting is carried out in two steps. The first step involves fitting plots of the conversion/dehydrated fraction (α) as a function of time from isothermal measurements to a variety of kinetic models in the following form.

$$\frac{d\alpha}{dt} = Ae^{-(E_a/RT)}f(\alpha) = k(T)f(\alpha) \quad (1)$$

where A is the pre-exponential (frequency) factor (min), E_a is the activation energy (kJ/mol), T is the absolute temperature (K), R is the gas constant ($8.314\,JK^{-1}\,mol^{-1}$), $k(T)$ is the rate constant, $f(\alpha)$ is the differential form of the reaction model, t is the time, and α is the conversion fraction. In practice, differential data, $d\alpha/dt$, are often quite noisy so that the integral version of Eq. (1), $g(\alpha)$, is used:

$$g(\alpha) = Ae^{-(E_a/RT)}t \quad (2)$$

where $g(\alpha)$ is the integral form of the reaction model.

For each reaction model, $g(\alpha)$ against time (t) plots are evaluated using various statistical parameters, such as the coefficient of regression line (R^2), the standard deviation of the slope of the regression line (S_b), the standard deviation of the regression line ($S_{y/x}$), and residual plots.[21,29] From these data, the kinetic model that provides the most acceptable fit is identified.

In the second step of model fitting, the natural logarithm of the slope of the regression line from the acceptable fit is plotted against the reciprocal of the absolute temperature, and Arrhenius parameters are calculated.

The model-fitting approach assumes constant E_a values over the entire reaction process. This assumption leads to unambiguous values of Arrhenius parameters that are likely to conceal multi-step kinetics.[30] Thus, use of model-free or isoconversional

Table 1. List of Solid-State Kinetics Models Used in This Study (Modified from Refs.[21,28])

Model	Differential Equation $f(\alpha) = 1/k(d\alpha/dt)$	Integral Equation $g(\alpha) = kt$	Mechanism
Nucleation models			
A2	$2(1-\alpha)[-\ln(1-\alpha)]^{1/2}$	$[-\ln(1-\alpha)]^{1/2}$	1D nuclei growth (Avrami–Erofeyev equation, $n=2$)
A3	$3(1-\alpha)[-\ln(1-\alpha)]^{2/3}$	$[-\ln(1-\alpha)]^{1/3}$	2D nuclei growth (Avrami–Erofeyev equation, $n=3$)
A4	$4(1-\alpha)[-\ln(1-\alpha)]^{3/4}$	$[-\ln(1-\alpha)]^{1/4}$	3D nuclei growth (Avrami–Erofeyev equation, $n=4$)
P1	$\alpha(1-\alpha)$	$\ln[\alpha/(1-\alpha)]+c$[a]	Random nucleation (Prout–Tompkins equation)
P2	$2\alpha^{1/2}$	$\alpha^{1/2}$	Power law ($n=1/2$)
P3	$3\alpha^{2/3}$	$\alpha^{1/3}$	Power law ($n=1/3$)
P4	$4\alpha^{3/4}$	$\alpha^{1/4}$	Power law ($n=1/4$)
Geometrical contraction models			
R2	$2(1-\alpha)^{1/2}$	$1-(1-\alpha)^{1/2}$	2D phase boundary reaction (contracting area)
R3	$3(1-\alpha)^{2/3}$	$1-(1-\alpha)^{1/3}$	3D phase boundary reaction (contracting volume)
Diffusion models			
D1	$1/(2\alpha)$	α^2	1D diffusion
D2	$-[1/\ln(1-\alpha)]$	$((1-\alpha)\ln(1-\alpha))+\alpha$	2D diffusion
D3	$[3(1-\alpha)^{2/3}]/[2(1-(1-\alpha)^{1/3})]$	$(1-(1-\alpha)^{1/3})^2$	3D diffusion (Jander equation)
D4	$3/[2((1-\alpha)^{-1/3}-1)]$	$1-(2/3)\alpha-(1-\alpha)^{2/3}$	3D diffusion (Ginstling–Brounshtein equation)
Reaction-order models			
R1	1	α	Zero-order reaction
F1	$(1-\alpha)$	$-\ln(1-\alpha)$	First-order reaction
F2	$(1-\alpha)^2$	$[1/(1-\alpha)]-1$	Second-order reaction
F3	$(1-\alpha)^3$	$(1/2)[(1-\alpha)^{-2}-1]$	Third-order reaction

methods have been suggested which are able to calculate E_a without theoretical assumptions. One suitable model-free approach for isothermal data is Friedman analysis, which is based on the logarithm of Eq. (1).

$$\ln\left(\frac{d\alpha}{dt}\right) = (\ln Af(\alpha)) - \frac{E_a}{RT} \quad (3)$$

According to this, a plot of $\ln(d\alpha/dt)$ versus $1/T$ at each α gives E_a from the slope for that α regardless of the model.[27]

However, it is worth mentioning that model-free methods do not allow the determination of a complete kinetic description of any solid-state reaction.[28] So, it is advisable to evaluate both model-fitting and model-free approaches, and analyze them to get better kinetic information. Moreover, it has been suggested to confirm kinetic interpretations with ancillary methods like microscopy.[24] Microscopy provides direct evidence of the step involved in the dehydration and may be useful to identify separate events such as nucleation and growth.

The most common methods for the study of dehydration kinetics include microscopy, differential scanning calorimetry (DSC), thermogravimetric analysis (TGA), and X-ray powder diffractometry (XRPD). The measurements from the aforementioned methods are converted to fraction dehydrated (α), which is then used in the kinetic analysis.

Nitrofurantoin (NF, Fig. 1) is a widely used antibiotic against many urinary tract infections. It is very slightly water soluble and falls in class IV of the biopharmaceutical classification system.[31] It exists as two anhydrate forms (α and β), two monohydrate forms (I and II), and at least two solvated forms.[32–36] Among all these forms, anhydrate β (NF-AH, CSD ref code: LABJON02) and monohydrate II (NF-MH, CSD ref code: HAXBUD) are the most common and reported ones so far. NF-AH to NF-MH transformation was observed during granulation and aqueous slurry experiments.[37] The transition from NF-AH to NF-MH during pelletization has also been reported, along with the conversion of the formed NF-MH back to NF-AH during the subsequent drying step.[9] This phenomenon exemplifies the need for a better mechanistic understanding of NF-MH dehydration which may contribute towards improving manufacturing process control. Some information exists on NF-MH dehydration, in which, dehydration has been studied using variable temperature X-ray diffraction.[38,39] The purpose of this study is to elucidate the dehydration kinetics of NF-MH using the concept of solid-state kinetics with model-fitting and model-free approaches. Furthermore, the kinetic interpretations are correlated with hot stage microscopy and XRPD information to gain a more reliable mechanistic understanding. Finally, the observed dehydration phenomenon is explained using available information on the crystal structure.

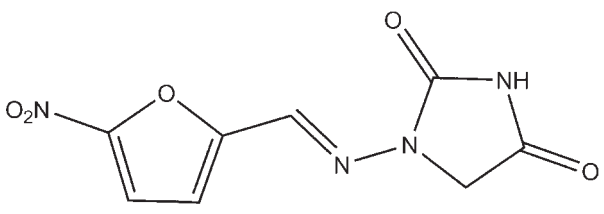

Figure 1. Molecular structure of nitrofurantoin.

MATERIALS AND METHODS

Nitrofurantoin (Ph. Eur. 5th Ed.) was obtained from Unikem, Copenhagen, Denmark (Lot no. 414072). It was found to correspond to the anhydrous β form of nitrofurantoin (CSD ref code: LABJON02) by XRPD and was used as received. For the preparation of monohydrate, acetone (Applichem, Darmstadt, Germany, lot no. 7H006456) and Mili-Q water were used.

Monohydrate Preparation

The received nitrofurantoin (2.150 g) was dissolved in 150 mL of acetone–water solution (volume ratio 1.5:1) in a 250 mL flask at 60°C. The solution was maintained at 60°C under stirring for 1 h to ensure complete dissolution of nitrofurantoin. Afterwards, the flask was kept in a water bath (Julabo SW23; Julabo Labortechnik GmBH, Seelbach, Germany) maintained at 50°C, and needle shaped crystal appeared within 24 h. Crystals were separated by vacuum filtration and were allowed to dry overnight under ambient conditions. Exposure to direct light was prevented during the entire work.

X-Ray Powder Diffraction (XRPD)

XRPD were measured on a PANalytical X'Pert PRO X-Ray Diffractometer (Almelo, The Netherlands) using a Cu Kα_1 radiation ($\lambda = 1.5406$ Å). The voltage and current were 45 kV and 40 mA, respectively. Samples were measured in reflection mode in the 2θ range 5–40° with a step size of 0.0334° 2θ using an X'celerator detector. Data were collected using X'Pert Data Collector software (PANalytical B.V.).

For isothermal XRPD measurements, sample was placed in a 0.2 mm deep holder, which was put in an Anton Paar CHC chamber (Anton Paar GmbH, Graz, Austria) mounted on the goniometer of the X-ray diffractometer. The temperature was raised from 25 to 120°C at a heating rate of 35°C/min using TCU 110 temperature controller (Anton Paar GmbH). Sample temperature was maintained at 120°C, and diffractograms were collected at every 5 min with a step size of

0.039° from 5 to 30° 2θ using a PIXcel detector. Each measurement time was 4 min and 51 s.

Differential Scanning Calorimetry (DSC)

DSC experiments were done using Perkin Elmer DSC 7 (Perkin Elmer, Norwalk, CT) controlled by Pyris software (version 7.0.0.0110). Two-point calibration using indium and tin was carried out to check the temperature axis and heat flow of the equipment. Samples were analyzed in 50 μL crimped pans having holes at 10°C/min under a nitrogen flow of 40 mL/min.

Thermogravimetric Analysis (TGA)

Isothermal dehydration studies were performed using a thermogravimetric analyzer (Perkin Elmer TGA 7) equipped with instrument control software (Pyris version 7.0.0.0110). The temperature was calibrated using the ferromagnetic standard, whereas weight calibration was performed using 100 mg standard. Samples (9.0 ± 0.5 mg) were analyzed in a flame-cleansed open platinum pan under a nitrogen purge of 40 mL/min.

Isothermal studies were performed at 11 different temperatures with a 1°C interval between 110 and 120°C, and each measurement was performed in triplicate. For each measurement, the furnace was heated rapidly at 100°C/min to reach the target temperature and maintained at that temperature isothermally until the completion of dehydration. The end of dehydration was judged when the weight was constant.

Hot-Stage Microscopy (HSM)

An Olympus BX50 microscope (Hamburg, Germany) coupled with a Linkam hot stage LTS350 (Linkam, Tadworth, Surrey, UK) and Pixelink PL-A662 digital camera was used for visualizing isothermal dehydration of NF-MH. Linksys 32 software (Linkam) was used for data acquisition and temperature control. The sample was placed on the hot stage, which was heated from 25 to 120°C at 30°C/min. The temperature was maintained at 120°C until the completion of dehydration was observed, and pictures were taken at every 60 s during the run under cross-polarized light.

Crystal Structure Visualization

The published crystal structures of nitrofurantoin were studied, and theoretical diffraction patterns were calculated based on single crystal X-ray analysis data using Mercury CSD 2.2 software (The Cambridge Crystallographic Data Centre, Cambridge, UK). The morphology prediction was done based on Bravais, Friedel, Donnay, and Harker (BFDH) theory, again using Mercury software.

Data Analysis

All calculations for the model-fitting approach were done with Microsoft® Office Excel 2003. The fraction dehydrated, α, was calculated from the TGA data using the following equation:

$$\alpha = \frac{W_0 - W_t}{W_0 - W_\infty} \tag{4}$$

where W_0, W_t, and W_∞ are the initial mass ($t = 0$), sample mass at time t, and the final sample mass ($t = \infty$), respectively. Various kinetic models given in Table 1 were fitted for the data from the $t = 5.0$ min to $\alpha = 0.9$. The fitted data were evaluated using various statistical parameters, and the most acceptable models were identified.

Friedman analysis, a model-free approach, was performed using commercial software, NETZSCH thermokinetic 3 (Netzsch GmbH, Selb, Germany, version 2008.05).

RESULTS AND DISCUSSION

The phase identification of prepared NF-MH was done using XRPD, TGA, and DSC. X-ray powder diffractograms of NF-MH obtained experimentally and calculated from the crystal structure data are shown in Figure 2. The experimental and calculated patterns correspond well, confirming that the crystallized form is a known monohydrate form II (CSD ref code: HAXBUD). Due to the preferred orientation, reflection intensities are not the same. The water content determined by TGA was 7.11% (w/w), which agrees with the theoretical water content of 7.03% (w/w). The dynamic TGA and DSC scan at 10°C/min showed dehydration occurring in single step within the range of 120–145°C (Fig. 3).

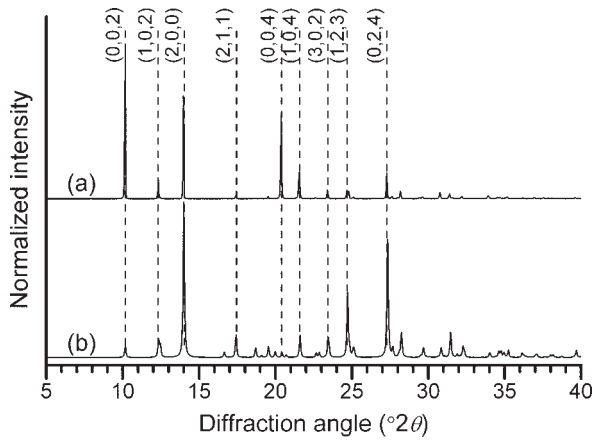

Figure 2. X-ray powder diffraction patterns of NF-MH (a) experimental (b) calculated from crystal structure data. Parentheses indicate hkl indices.

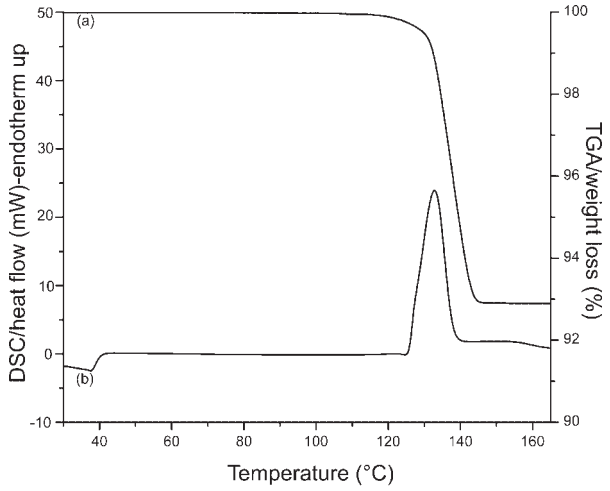

Figure 3. (a) TGA and (b) DSC thermograms of NF-MH under nonisothermal conditions.

Isothermal Dehydration and Model-Fitting Analysis

Various factors such as particle size, particle shape, and sample mass affect the isothermal dehydration results obtained using TGA.[22,29] Particle size could be controlled by taking a particular sieve fraction for the dehydration studies. However, sieving invariably creates breakage of particles, which could lead to formation of crystal defects and nucleation sites. Dehydration usually begins at crystal defects, where molecules are more energetic due to lattice strain. Sieving induced crystal defects may thus conceal actual dehydration or may markedly affect the rate of it.[25] Considering this, sieving was avoided, and original unfractioned particles were used.

Typical isothermal dehydration plots for the NF-MH dehydration are shown in Figure 4. The fraction dehydrated (α) was calculated using Eq. (4). At all the temperatures studied, the shape of the curve is sigmoidal, indicating an initial short induction period at low-α values, an acceleratory period at intermediate α values, and finally a decay period at high-α values. The sigmoidal plot usually results from reactions that occur at a reactant–product interface.[16] The interface is initially established as a limited number of points on the surface of the reactant crystals by formation of microcrystals (nuclei) of the product. Reaction thereafter proceeds within the strained area at the reactant–product interface. At the start of the reaction, the area of such an interface is small and limited to a number of surface sites so that the reaction is slow. As the reaction proceeds, some nuclei start growing and new nuclei are also formed, and thus, the reaction rate starts to increase. The continuous nuclei growth and coalescence during the end part of the reaction causes a decrease in reactant–product interface and the reaction rate.

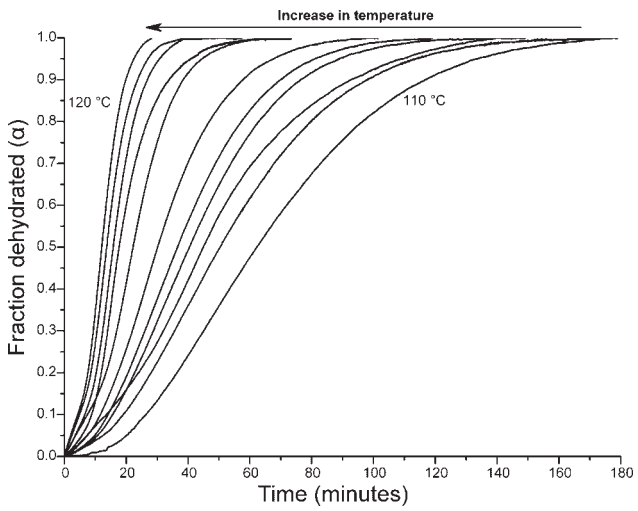

Figure 4. Representative isothermal dehydration progress curves of NF-MH.

It is advisable to analyze solid-state kinetics over selected conversion values because errors are usually higher at very low and high conversion values.[40] Therefore, model fitting was performed on the data from the $t = 5.0$ min to $\alpha = 0.9$, and data were fitted to the integral form, $g(\alpha)$ of the kinetic models listed in Table 1. To identify an acceptable fit, various statistical parameters, R^2, S_b, $S_{y/x}$, and residual plots for each model were evaluated. The results from this first step of model-fitting are given in Table 2.

The dehydration kinetics is best described by model A2, Avrami–Erofeyev Equation ($n = 2$) with no trend in residuals. However, statistical parameters for other models, A3, A4, R2, and R3, also indicated a good fit for the dehydration data and identification of the most appropriate kinetic model was not feasible. Model-fitting analysis often indicates several models appropriately explaining the reaction kinetics, and unambiguous identification of the single most suitable model becomes difficult.[19,23,41,42] Nevertheless, it can be still inferred from model-fitting that the dehydration of NF-MH proceeds by nucleation–growth and/or geometric contraction mechanisms. Further evaluation of the most probable dehydration mechanism was done based on microscopic observations and model-free analysis, and is discussed later.

Arrhenius parameters calculated for all models are listed in Table 3. The values of activation energy derived from each model are not significantly different, while the obtained frequency factor differs among the models. It is often the case with model-fitting that several models approximate the similar value of activation energy.[19,23,27,42] The activation energy ranged from about 196–213 kJ/mol for statistically suitable models (A2, A3, A4, R2, and R3).

Table 2. Statistical Parameters of Fitting Isothermal Dehydration of Nitrofurantoin Monohydrate.

	A2	A3	A4	P1	P2	P3	P4	R2	R3	D1	D2	D3	D4	R1	F1	F2	F3
R^2	**0.9956**	**0.9883**	**0.9800**	0.9780	0.9501	0.9285	0.9151	**0.9892**	**0.9853**	0.9652	0.9427	0.8946	0.9287	0.9817	0.9659	0.8224	0.6348
$S_{y/x}$	**0.0212**	**0.0264**	**0.0280**	0.1823	0.0443	0.0437	0.0401	**0.0198**	**0.0182**	0.0449	0.0458	0.0260	0.0152	0.0322	0.1073	0.8469	5.7364
S_b	**0.0001**	**0.0001**	**0.0001**	0.0004	0.0001	0.0001	0.0001	**0.0001**	**0.0000**	0.0001	0.0001	0.0001	0.0000	0.0001	0.0003	0.0026	0.0181

R2, the mean value of correlation coefficient for the linear regression of the $g(\alpha)$ versus t plot; Sy/x, the mean value of standard deviation of the linear regression of the $g(\alpha)$ versus t plot; Sb, the mean value of standard deviation of the slope for the linear regression of the $g(\alpha)$ versus t plot.
All parameters are average of three independent measurements. The statistical parameters of best fitting models are in bold.

Model-Free Analysis

The main impetus for using model-free or isoconversional methods is to overcome the implicit assumption of model-fitting analysis on constant activation energy over the entire reaction. Model-free analysis permits determination of the dependence of activation energy on the extent of conversion. Thus, a complementary approach of using model-fitting and model-free methods together permits more reliable evaluation of reaction kinetics and activation energy.

In this study, model-free analysis was carried out using Friedman's isoconversional method. Kinetic analysis done with Friedman isoconversional method has shown lower variation in the activation energy compared to the standard isoconversional method.[40] Figure 5 gives a Friedman analysis plot for NF-MH dehydration showing variation of activation energy, E_a, as a function of conversion, α. The activation energy for the entire range of α in Figure 5 is about 170–230 kJ/mol (95% confidence interval), which corresponds well with all acceptable models (A2, A3, A4, R2, and R3) from model-fitting analysis. This match in activation energy derived from model-fitting and model-free analysis indicates the reliability of both these methods for evaluation of dehydration kinetics.

The E_a values are slightly higher in the Friedman's analysis at initial α values ($\alpha \leq 0.20$), and then remain approximately constant for the later dehydration process. This higher activation energy during the early stage of dehydration could be attributed to nucleation of the product phase. A similar trend was also observed during the dehydration of piroxicam monohydrate and nedocromil sodium trihydrate.[21,23] The large variation in activation energy during the process is usually due to a complex dehydration mechanism, where multiple reactions occur simultaneously. In the dehydration of NF-MH, the activation energy remains fairly constant, and thus the reaction can be postulated to be a simple single step process.

Table 3. Activation Energy (E_a) and Frequency Factors (A) from Arrhenius Plots Derived using Model Fitting Approach

Model	E_a (kJ/mol)[a]	$\ln A$ (min)[a]
A2	211.9 ± 11.1	59.8 ± 2.0
A3	196.7 ± 8.0	57.3 ± 2.3
A4	197.7 ± 13.2	57.1 ± 3.6
P1	187.2 ± 7.5	56.0 ± 2.2
P2	190.3 ± 11.1	55.1 ± 3.3
P3	182.7 ± 11.7	52.4 ± 3.5
P4	178.2 ± 11.9	50.9 ± 3.5
R2	211.7 ± 6.4	61.6 ± 1.8
R3	213.6 ± 5.6	62.0 ± 1.5
D1	218.9 ± 4.7	64.1 ± 1.3
D2	221.7 ± 3.1	64.7 ± 0.7
D3	224.8 ± 1.2	64.8 ± 0.2
D4	222.8 ± 2.4	63.8 ± 0.5
R1	205.6 ± 8.9	60.0 ± 2.6
F1	217.2 ± 4.0	64.5 ± 1.0
F2	226.1 ± 0.3	68.4 ± 0.3
F3	231.9 ± 3.0	71.6 ± 1.2

[a]Mean ± standard deviation, $n = 3$.

Isothermal HSM and XRPD

The direct microscopic observations provide essential geometric information to identify and substantiate the most satisfactory kinetic model obtained from isothermal dehydration data.[24,25] This is particularly important because solid-state kinetics models are based on geometric model functions, and therefore results from these models can be verified by visual observation of the dehydration reaction. Knowledge of the initial interface development and its progressive

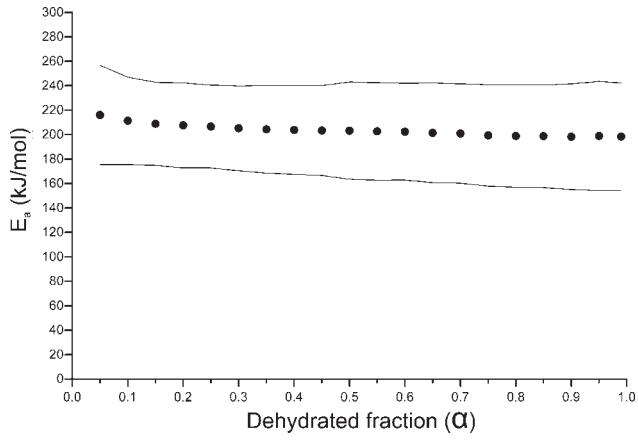

Figure 5. Friedman analysis plot showing dependence of activation energy (E_a) on fraction dehydrated (α). The upper and lower lines define 95% confidence levels.

growth gained from microscopy provides a basis for meaningful and unambiguous interpretation of the kinetic data.

Photomicrographs taken during isothermal dehydration of NF-MH at 120°C using hot stage microscopy are shown in Figure 6. The NF-MH crystal exhibited strong birefringence under cross-polarized light, and it is oriented in parallel direction to the (0 0 2) face. It should be noted that, in comparison to the calculated BFDH morphology shown in Figure 7, the obtained crystals have preferentially grown in the direction of the (1 1 1) and (1 −1 1) face, and thus a larger (0 0 2) face is observed. This is also apparent in the XRPD (Fig. 2), in which the experimental pattern shows a higher intensity at 10.1°2θ (corresponding to the (0 0 2) face) due to a substantial preferred orientation. During the time to reach the target temperature (about 3 min), no visible change was observed in the sample, indicating that dehydration had not been initiated before the isothermal temperature was reached. The first signs of nuclei formation were observed within 2 min at 120°C, which can be seen as the appearance of tiny dark spots on the NF-MH crystal. Dehydration initiates nuclei formation mainly on the (0 0 2) and (1 0 2) faces. It was not possible to visualize the effect of the dehydration on the other faces, such as (1 1 1), due to their considerable thickness and smaller area. However, it can be postulated that dehydration would start on the entire surface of the crystal and that similar nuclei formation occurs on the (1 1 1) face. With respect to solid-state kinetics, these initial nuclei most probably represent the germ/growth nuclei. As a precursor of them, incipient nuclei, defined as a modified or somewhat activated site on the reactant, may not be accessible to experimental detection under most conditions.[43] From each nuclei, the propagation of a dehydration reaction is visible along two directions, the *a*-axis and the *b*-axis. The advancing nuclei growth is essentially planar on the product surface, exhibiting an approximately two-dimensional growth, and thus rule out the suitability of model A2 (one-dimensional nuclei growth) to describe NF-MH dehydration. However, to achieve complete dehydration the reaction front also has to migrate towards the inner region at some stage during the progress, giving three-dimensional nuclei growth. For many dehydration reactions fitting to the Avrami–Erofeyev equation, A2 ($n = 2$) have been reported, which does not concede with microscopic evidence, suggesting that the nuclei grew in three directions.[25] Although inner migration of the interface (third dimension) was not observed during NF-MH dehydration, its occurrence cannot be neglected from the theoretical perspective. Thus, overall both model A3 and A4 can be considered to be well suited to

Figure 6. Dehydration of NF-MH observed during isothermal polarized hot stage microscopy at 120°C. Crystal axes and hkl indices are indicated in the upper left figure.

 DOI 10.1002/jps

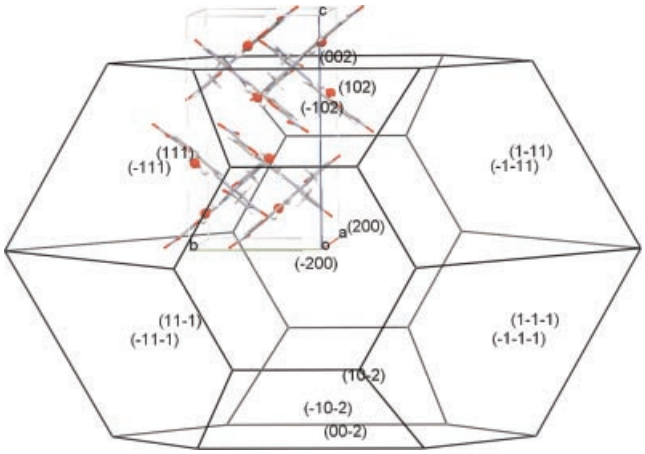

Figure 7. Calculated BFDH morphology of NF-MH crystal.

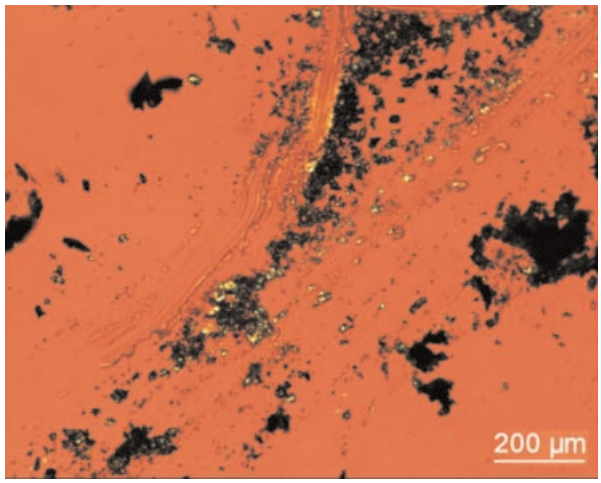

Figure 8. Photomicrograph of the broken dehydration product of NF-MH.

explain NF-MH dehydration kinetics. In solid-state reactions, nuclei growth is confined by two restrictions, ingestion or coalescence.[28] Ingestion is the elimination of a potential nucleation site by growth of an existing nucleus, while coalescence involves loss of reactant/product interface with the merging of two or more growing nuclei. Microscopic observations in Figure 6 suggest coalescence of nuclei during NF-MH dehydration. The question regarding the acceptability of R2 and R3 models (geometrical contraction) based on model-fitting was also addressed by microscopy. It was observed during the later stage of dehydration that, due to coalescence of nuclei, the reaction front takes the shape of a contracting envelope. This is the secondary phenomenon occurring due to nuclei growth, and due to which R2 and R3 also gave a satisfactory fit.

The knowledge about the dehydration end product is imperative to determine consequences associated with the loss of water from the hydrate crystal. After the completion of NF-MH dehydration, birefringence was no longer observed, and the crystal appeared opaque under polarized light. This could be due to the formation of either amorphous or polycrystalline product. To confirm this, the crystal was gently broken after the completion of dehydration, and was observed under the microscope (Fig. 8). The broken fragments showed birefringence indicating their crystalline nature. This could be due to the fact that final product is an assemblage of microcrystals (polycrystalline) having substantially less crystallinity and are thus not able to give birefringence. This phenomenon is common during dehydration, where crystals may become polycrystalline due to a change in density or a rearrangement of the crystal structure.[44] In two reported studies on dehydration of NF-MH using variable temperature XRPD (VT-XRPD), the substantial loss of peak intensity was observed after 120°C indicating a decrease in crystallinity, and the final solid form after dehydration was found to be NF-AH (anhydrous β form).[38,39] We monitored dehydration using isothermal XRPD measurements in which sample was kept at 120°C and diffractograms were measured at different time points. This condition is closer to the TGA and HSM experiments of this study, which should provide a better comparison of the dehydration observed using these different techniques.

The results from isothermal XRPD measurements are shown in Figure 9. In comparison with XRPD pattern at 25°C, initial diffractogram at 120°C shows a shift of peaks towards lower angles (higher d spacing), which could be attributed to temperature-induced lattice expansion. Initiation of dehydration is observed by appearance of a new peak at 14.2° 2θ.

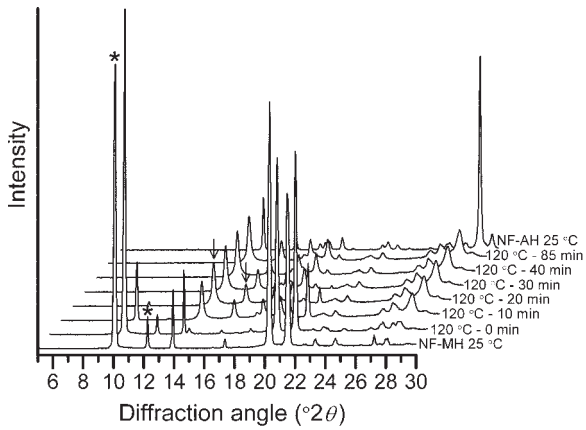

Figure 9. Waterfall plot showing XRPD profiles of NF-MH during isothermal dehydration at 120°C. Characteristic peaks of NF-MH and NF-AH are marked with asterisk and arrow, respectively.

Within 10 min at 120°C, several new peaks at 16.4, 18.3, 19.5, and 26.2° 2θ were also observed. The intensities of these peaks increased with time, and a simultaneous decrease in peak intensity at 9.9, 18.3, 20.0, and 21.2° 2θ was observed. The dehydration was finished in 40 min, and no change in diffractogram was observed until 85 min. All new peaks correspond to NF-AH (β-form), and the final diffractogram at 85 min also correspond well with the NF-AH diffractogram. Afterwards, heating the sample at 10°C/min showed higher peak intensities with increases in temperature (data not shown). This indicates that the crystallinity of the anhydrate product increases at higher temperature. Overall, these data indicates that NF-MH on dehydration remains crystalline and reorganizes in anhydrate β structure. During the experiments, no intermediate amorphous phase was observed (within the detection limit of the XRPD method). Microscopic observations showing microcrystals after dehydration are also in agreement with VT-XRPD data. It was also possible to classify NF-MH dehydration according to the scheme proposed by Galwey.[25] Based on this scheme, NF-MH dehydration proceeds according to WET3 (Water Evolution Type 3) class, which explains dehydration based on interface advance due to nucleation–growth or contracting envelope. In the case of NF-MH, WET3 is followed by a nucleation and growth mechanism in which the initial nucleation is rapid and accompanied by a positive tendency to form coalescence with neighboring nuclei.

Dehydration Correlation With the Crystal Structure

The crystal structures of the NF-MH and two anhydrates, α (CSD ref code: LABJON01) and β (CSD ref code: LABJON02), were studied to understand the effect of the removal of the water molecules from the NF-MH. The planar conformation of the NF molecule is essentially similar among these forms.

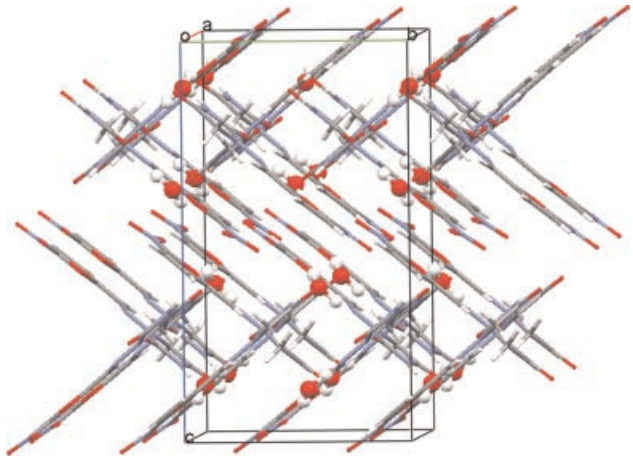

Figure 10. Projection of NF-MH crystal structure along the *a*-axis. Water molecules are shown in ball-stick style for visual clarity.

The crystal structure of NF-MH determined by Pienaar et al.[33] reveals that water molecules are not accommodated in the form of channels, layers or tunnels. In fact, water molecules are located in isolated cavities within the herring-bone arrangement of nitrofurantoin molecules (Fig. 10). In the asymmetric unit of NF-MH, the nitrofurantoin molecule is coplanar with the atoms of the water molecule. Each water molecule links two nitrofurantoin molecules by hydrogen bonds having moderate strength (Fig. 11a). Based on the model proposed by Petit and Coquerel,[26] the first step during dehydration involves removal of the water molecules from the hydrate structure. Various studies concerning hydrates with channels/tunnels have shown preferential escape of water molecules in the direction of channels with anisotropic dehydration.[5,20,45] In the case of NF-MH, this type of unidirectional and smooth water loss is likely to be impeded by the NF molecules.

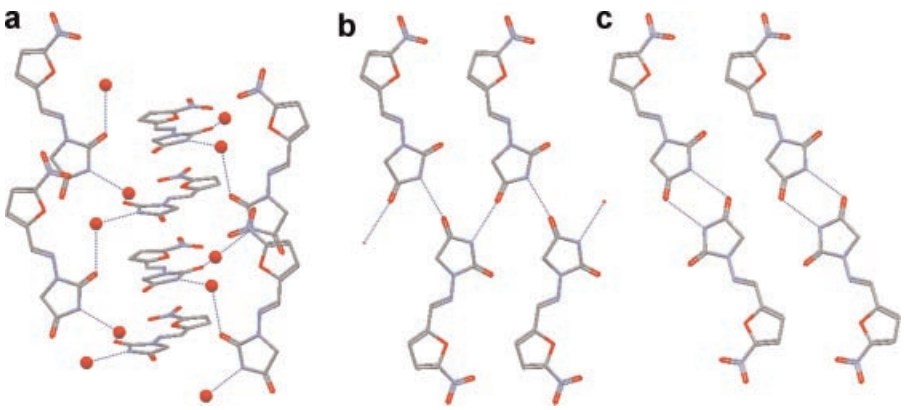

Figure 11. Hydrogen bond interactions in (a) NF–MH, (b) NF–AH, β-form, and (c) α-form. Nitrofurantoin molecules and water molecules are shown in capped stick and ball-stick, respectively. Hydrogen atoms are removed for clarity.

 DOI 10.1002/jps

This may explain the higher dehydration activation energy for NF-MH, even though the hydrogen bond interactions are not strong. The initiation of dehydration can only start when water molecules have gained sufficient energy to come out of the complicated molecular arrangement. In the beginning, nuclei would be formed at several places on the crystal surface that provide the most suitable route of escape for water molecules. Afterwards, dehydration would proceed by removal of water molecules lying near the initial nuclei, thus promoting nuclei growth. Furthermore, the release of water molecules is expected to create a local collapse of the crystal lattice. However, it should be noted that no amorphous phase was observed during the isothermal XRPD measurements, which might be due to the very fast structural reorganization to the crystalline phase. The reorganization of the dehydrated phase could lead to formation of any of the anhydrate forms. The two anhydrate forms of NF, α and β have similar packing energy and stability.[32] Thus, reorganization to each of these forms is equally possible from the thermodynamic perspective. However, current study, as well as all reported data on the NF-MH dehydration, have shown formation of the β form only.[32,38,39] In both anhydrates, NF molecules are packed in layers, indicating lack of structural similarity to the herring-bone arrangement in the NF-MH structure. Figure 11 shows hydrogen bond motifs of NF-MH and both anhydrates. The principal N–H···O hydrogen bond interaction is common in both anhydrates, but provides different molecular association and crystal structures. In the case of the α form, the NF molecules are associated in a "head-to-head" arrangement forming dimers, whereas for the β form, NF molecules are related by the twofold screw-axis with each molecule interacting with two other molecules. After release of the water molecules, breakage of hydrogen bonds, and creation of void spaces in the crystal lattice would enable NF molecules to undergo packing changes. It appears that packing changes/molecular translations favor the formation of hydrogen bond interactions of the β form over the α form. Overall, it can be concluded that NF-MH undergoes destructive dehydration, and that the dehydrated product subsequently reorganizes to the β form. Thus, the dehydration can be attributed to follow class I-destructive–reconstructive from the scheme of Petit and Coquerel.

CONCLUSIONS

The dehydration of NF-MH was studied using model-fitting and model-free analysis. Several acceptable models giving similar activation energy were obtained from the model-fitting approach. The kinetic fit evaluation suggested that dehydration proceeds by nucleation–growth and/or geometrical contraction of reactant–product interface. This ambiguity was resolved from the results of dehydration observed during HSM. Microscopic observations clearly showed that the dehydration occurs with a rapid nucleation, which is followed by two/three-dimensional nuclei growth and coalescence. Based on this, dehydration was attributed to follow the Avrami–Erofeyev equation with $n = 3$ or 4 (model A3 and A4). The activation energy value from model-free analysis was consistent with the results obtained from these models. Both methods gave an average activation energy of about 196–197 kJ/mol, which is relatively high compared to other pharmaceutical hydrates studied to date. It was concluded that NF-MH dehydration occurs in the single step with the formation of poorly crystalline NF-AH. The higher activation energy is attributed to the complex crystal structure in which water molecules cannot easily escape. The combined approach of using model-fitting and model-free analysis complemented by HSM and XRPD was found to be a valuable methodology to obtain a precise understanding of dehydration behavior.

ACKNOWLEDGMENTS

The Drug Research Academy (Copenhagen, Denmark) and H. Lundbeck A/S are thanked for the financial support. The grant from Lundbeckfonden (Copenhagen, Denmark) for the purchase of X-ray powder diffractometer is greatly acknowledged (grant decision 479/06). Netzsch GmbH is thanked for providing evaluation copy of the thermokinetic software.

REFERENCES

1. Griesser UJ. 2006. The importance of solvates. In: Hilfiker R, editor. Polymorphism in the pharmaceutical industry. Weinheim: Willey-VCH Verlag GmbH & Co. pp 211–233.
2. Morris KR. 1999. Structural aspects of hydrates and solvates. In: Brittain HG, editor. Polymorphism in pharmaceutical solids. New York: Marcel Dekker, Inc. pp 125–182.
3. Brittain HG. 2008. Polymorphism and solvatomorphism 2006. J Pharm Sci 97:3611–3636.
4. Brittain HG. 2009. Polymorphism and solvatomorphism 2007. J Pharm Sci 98:1617–1642.
5. Byrn SR, Pfeiffer RR, Stowell JG. 1999. Solid-state chemistry of drugs, 2nd edition. West Lafayette, IN: SSCI, Inc. pp 233–247.
6. Garner WE. 1955. Chemistry of solid state. London: Butterworths Scientific Publications. pp 213–231.
7. Variankaval N, Lee C, Xu J, Calabria R, Tsou N, Ball R. 2007. Water activity-mediated control of crystalline phases of an active pharmaceutical ingredient. Org Process Res Dev 11: 229–236.

8. Wikström H, Marsac PJ, Taylor LS. 2005. In-line monitoring of hydrate formation during wet granulation using Raman spectroscopy. J Pharm Sci 94:209–219.
9. Sandler N, Rantanen J, Heinamaki J, Romer M, Marvola M, Yliruusi J. 2005. Pellet manufacturing by extrusion-spheronization using process analytical technology. AAPS PharmSciTech 6:E174–E182.
10. Hausman DS, Cambron RT, Sakr A. 2005. Application of on-line Raman spectroscopy for characterizing relationships between drug hydration state and tablet physical stability. Int J Pharm 299:19–33.
11. Aaltonen J, Kogermann K, Strachan CJ, Rantanen J. 2007. In-line monitoring of solid-state transitions during fluidisation. Chem Eng Sci 62:408–415.
12. Leung SS, Padden BE, Munson EJ, Grant DJW. 1998. Solid-state characterization of two polymorphs of aspartame hemihydrate. J Pharm Sci 87:501–507.
13. Cavatur RK, Suryanarayanan R. 1998. Characterization of phase transitions during freeze-drying by in situ X-ray powder diffractometry. Pharm Dev Technol 3:579–586.
14. Higgins JP, Arrivo SM, Reed RA. 2003. Approach to the determination of hydrate form conversions of drug compounds and solid dosage forms by near-infrared spectroscopy. J Pharm Sci 92:2303–2316.
15. Jørgensen AC, Strachan CJ, Pollanen KH, Koradia V, Tian F, Rantanen J. 2009. An insight into water of crystallization during processing using vibrational spectroscopy. J Pharm Sci 98:3903–3932.
16. Sheng J, Venkatesh GM, Duddu SP, Grant DJ. 1999. Dehydration behavior of eprosartan mesylate dihydrate. J Pharm Sci 88:1021–1029.
17. Niazi S. 1978. Thermodynamics of mercaptopurine dehydration. J Pharm Sci 67:488–491.
18. Shefter E, Fung HL, Mok O. 1973. Dehydration of crystalline theophylline monohydrate and ampicillin trihydrate. J Pharm Sci 62:791–794.
19. Dong ZD, Salsbury JS, Zhou DL, Munson EJ, Schroeder SA, Prakash I, Vyazovkin S, Wight CA, Grant DJW. 2002. Dehydration kinetics of neotame monohydrate. J Pharm Sci 91: 1423–1431.
20. Perrier PR, Byrn SR. 1982. Influence of crystal packing on the solid-state desolvation of purine and pyrimidine hydrates: Loss of water of crystallization from thymine monohydrate, cytosine monohydrate, 5-nitrouracil monohydrate, and 2′-deoxyadenosine monohydrate. J Org Chem 47:4671–4676.
21. Sheth AR, Zhou D, Muller FX, Grant DJ. 2004. Dehydration kinetics of piroxicam monohydrate and relationship to lattice energy and structure. J Pharm Sci 93:3013–3026.
22. Taylor LS, York P. 1998. Effect of particle size and temperature on the dehydration kinetics of trehalose dihydrate. Int J Pharm 167:215–221.
23. Zhou D, Schmitt EA, Zhang GGZ, Law D, Wight CA, Vyazovkin S, Grant DJW. 2003. Model-free treatment of the dehydration kinetics of nedocromil sodium trihydrate. 92:1367–1376.
24. Galwey AK, Koga N, Tanaka H. 1990. A kinetic and microscopic investigation of the thermal dehydration of lithium-sulfate monohydrate. J Chem Soc Faraday Trans 86:531–537.
25. Galwey AK. 2000. Structure and order in thermal dehydrations of crystalline solids. Thermochim Acta 355:181–238.
26. Petit S, Coquerel G. 1996. Mechanism of several solid–solid transformations between dihydrated and anhydrous copper(II) 8-hydroxyquinolinates. Proposition for a unified model for the dehydration of molecular crystals. Chem Mater 8:2247–2258.
27. Khawam A, Flanagan DR. 2006. Basics and applications of solid-state kinetics: A pharmaceutical perspective. J Pharm Sci 95:472–498.
28. Khawam A, Flanagan DR. 2006. Solid-state kinetic models: Basics and mathematical fundamentals. J Phys Chem B 110: 17315–17328.
29. Agbada CO, York P. 1994. Dehydration of theophylline monohydrate powder—effects of particle-size and sample weight. Int J Pharm 106:33–40.
30. Vyazovkin S, Wight CA. 1999. Model-free and model-fitting approaches to kinetic analysis of isothermal and nonisothermal data. Thermochim Acta 341:53–68.
31. Kasim NA, Whitehouse M, Ramachandran C, Bermejo M, Lennernas H, Hussain AS, Junginger HE, Stavchansky SA, Midha KK, Shah VP, Amidon GL. 2004. Molecular properties of WHO essential drugs and provisional biopharmaceutical classification. Mol Pharm 1:85–96.
32. Caira MR, Pienaar EW, Lötter AP. 1996. Polymorphism and pseudopolymorphism of the antibacterial nitrofurantoin. Mol Cryst Liq Cryst 279:241–264.
33. Pienaar EW, Caira MR, Lötter AP. 1993. Polymorphs of nitrofurantoin.1. Preparation and X-ray crystal-structures of two monohydrated forms of nitrofurantoin. J Crystallogr Spectr Res 23:739–744.
34. Pienaar EW, Caira MR, Lötter AP. 1993. Polymorphs of nitrofurantoin. 2. Preparation and X-ray crystal-structures of two anhydrous forms of nitrofurantoin. J Crystallogr Spectr Res 23:785–790.
35. Tian F, Baldursdóttir S, Rantanen J. 2009. Effects of polymer additives on the crystallization of hydrates: A molecular-level modulation. Mol Pharm 6:202–210.
36. Tian F, Qu H, Louhi-Kultanen M, Rantanen J. Crystallization of a polymorphic hydrate system. J Pharm Sci 99:753–763.
37. Wikström H, Rantanen J, Gift AD, Taylor LS. 2008. Toward an understanding of the factors influencing anhydrate-to-hydrate transformation kinetics in aqueous environments. Cryst Growth Des 8:2684–2693.
38. Karjalainen M, Airaksinen S, Rantanen J, Aaltonen J, Yliruusi J. 2005. Characterization of polymorphic solid-state changes using variable temperature X-ray powder diffraction. J Pharm Biomed Anal 39:27–32.
39. Kishi A, Otsuka M, Matsuda Y. 2002. The effect of humidity on dehydration behavior of nitrofurantoin monohydrate studied by humidity controlled simultaneous instrument for X-ray diffractometry and differential scanning calorimetry (XRD-DSC). Colloids Surf B 25:281–291.
40. Khawam A, Flanagan DR. 2005. Role of isoconversional methods in varying activation energies of solid-state kinetics—I. Isothermal kinetic studies. Thermochim Acta 429:93–102.
41. Vyazovkin S, Wight CA. 1997. Kinetics in solids. Annu Rev Phys Chem 48:125–149.
42. Zhou DL, Grant DJW. 2004. Model dependence of the activation energy derived from nonisothermal kinetic data. J Phys Chem A 108:4239–4246.
43. Galwey AK, Laverty GM. 1990. The nucleus in solid-state reactions—Towards a definition. Solid State Ionics 38:155–162.
44. Nichols G. 2006. Light microscopy. In: Hilfiker R, editor. Polymorphism in the pharmaceutical industry. Weinheim: Willey-VCH Verlag GmbH & Co. pp 167–209.
45. Byrn SR, Lin CT. 1976. The effect of crystal packing and defects on desolvation of hydrate crystals of caffeine and L-(-)-1,4-cyclohexadiene-1-alanine. J Am Chem Soc 98:4004–4005.